A Comparison of Three Turbulence Models in Engine-Like Geometries

S. H. El-Tahry
Fluid Mechanics Department
General Motors Research Labs
12m S Mound Roads
Warren, Michigan 48090

ABSTRACT

Three turbulence models, namely the Reynolds stress model (RSM), the k-ϵ model, and a constant diffusivity model (CDM), were used in a comparative study to assess their accuracy in calculating in-cylinder fluid motions in axisymmetric engine geometries. To reduce numerical errors to a minimum, the skew upwind differencing scheme and the quadratic upstream interpolation for convection kinematics scheme were tested, and the most accurate of the two was used in the comparison between the turbulence models. The models were tested by considering a flow field generated in an axisymmetric piston-cylinder assembly. Both swirling and non-swirling flows were examined. The comparisons suggests that the RSM results are generally in better agreement with the experimental data than the k-ϵ model results. By proper tuning of the diffusivity, the CDM, which predicts only the mean flow, could be made to yield good agreement with the measurements. However, this could be achieved at only one of the two crank angles where comparisons with measurements were made.

INTRODUCTION

With the great advances occurring in the area of electronic computers, there is a continuing trend towards using computational techniques for aiding in the design of engineering equipment. This trend has diversified into many areas and currently computational techniques are starting to be used for exploring transport and combustion processes occurring in internal combustion engines (ICE's). The impact of such explorations on the development of ICE's depends on, among other things, the adequate representation of turbulence (via a turbulence model in multi-dimensional methods) in the computational procedure.

Several types of turbulence models are currently being used in engine applications. The commonly used ones are the constant diffusivity model and the two-equation turbulence model [1]. More recently a Reynolds stress model was also employed [2]. With several such models now available, an immediate question that arises is, which of these models is most appropriate for ICE applications? No simple answer is available as several factors need to be considered. Examples of such factors are complexity of the model, computer facility, cost of development, and accuracy of the solution. In deciding on the most appropriate model to use, each of the mentioned factors has a different "weight" that depends on the needs of, and constraints on, the user. The present work addresses the relative accuracy of three different models.

Previously, quantitative assessment of a two-equation (one for the turbulence kinetic energy (k), and the other for the dissipation rate of k (ϵ)) turbulence model was made by Gosman et al. [3], Diwakar and El Tahry [4], Ahmadi-Befrui et al. [5] and Ramos et al. [6]. In the former two works, the model results were compared to the measurements of Morse et al. [7]. The measurements used in the comparisons were made for non-swirling flow generated in an axisymmetric, non-compressing piston cylinder assembly. Ahmadi-Befrui et al. [5] and Ramos et al. [6] compared their model results to measurements also made in a non-swirling axisymmetric flow, but in this case, compression was considered. Recently, El Tahry [2] calculated the same flow field as in [3] and [4] while using a Reynolds stress model (RSM). These calculations yielded better agreement with the measurements than either of the two calculations made with the k-ϵ turbulence model. However, because the calculations of [2] were conducted with a different numerical differencing scheme than used in earlier works,[1] it was suspected that part of the improvement could be a consequence of the numerical scheme and not just the turbulence model.

Therefore, in order that a valid comparison between the turbulence models is achieved,

1. None of these works had ensured a grid independent solution.

numerical inaccuracies should be reduced to a minimum, and the same numerical procedure should be used in the calculations employing the different turbulence models.

Reduction of numerical errors can be achieved by grid refinements. However, due to the rapid increase in computation time which occurs when a grid is refined, there are obviously limits to this procedure. The alternative is to use more accurate differencing schemes. Two such schemes have been proposed - one by Raithby [8], which is the skew-upwind differencing scheme (SUDS). The other scheme is the quadratic upstream interpolation for convective kinematics (QUICK) scheme proposed by Leonard [9]. These two differencing schemes were previously employed by several authors [10-13], and results obtained with them clearly indicated that they were more accurate than the commonly used upwind differencing scheme (UDS).

The work presented herein is mainly a comparative study between the performance of the k-ϵ model and the Reynolds stress model in engine-type flows. A constant diffusivity model (CDM) is also included in the comparison, but it is included in only one of the two flow cases considered. Initially, both SUDS and QUICK were used to determine which of them was most appropriate for the present application. It was found that SUDS gives results in better agreement with the measured data and; therefore, it was used in the comparative study between the turbulence models.

In spite of using SUDS, it was still necessary, in order to approach a grid independent solution, to utilize fine computational meshes in the solution procedure. Consequently, the computer times required were substantial, and it was necessary to find means of reducing these computational times. Because of the specific solution procedure employed [13], it was possible to reduce computational times by appropriate variations in the computational engine motoring speed. The validity of this approach rests on the assumption of dynamic similarity which was found to be valid in the present flow situation.

The measurements used to compare with the model results are those made by Morse et al. [7]. Unlike earlier works which used these measurements in their comparisons, in the present study the comparison with measurements is extended to include one of the swirling flow cases reported in [7].

ANALYSIS

Governing Equations and Numerical Aspects

Governing Equations. The flow considered here is, for all practical purposes, incompressible and isothermal. The governing transport equations required for calculating the mean flow are the conservation equations of mass and momentum. For brevity and generality, these are expressed in general curvilinear coordinates as follows:

$$\overline{U^j}_{,j} = 0 \qquad (1)$$

$$\frac{\partial \overline{U^i}}{\partial t} + (\overline{U^i U^j})_{,j} = -\frac{1}{\rho} g^{ij} \overline{P}_{,j} + (\nu g^{jk} \overline{U^i}_{,k})_{,j} - (\overline{u^i u^j})_{,j} \qquad (2)$$

where U^m and u^m are, respectively, the instantaneous and turbulent contravariant velocity components, P is the pressure, ν is the kinematic viscosity, ρ is the density, t is time, and g^{ij} is the contravariant component of the unit tensor. The ",j" signifies covariant differentiation with respect to the j coordinate, and the overbars indicate ensemble averages. In Equations (1) and (2) and in what follows, indices repeated diagonally (i.e., once as a superscript and once as a subscript) imply summation.

Within the framework of the k-ϵ model (an eddy diffusivity model), the Reynolds stress contravariant component $\rho u^i u^j$ (appearing in Equation (2) divided by ρ) is calculated from:

$$\overline{\rho u^i u^j} = \mu_t (g^{mj} \overline{U^i}_{,m} + \overline{U^j}_{,m} g^{mi}) - \frac{2}{3} k g^{ij} \qquad (3)$$

where μ_t is the turbulent diffusivity. In the case of the k-ϵ model, μ_t is calculated from:

$$\mu_t = 0.09 \frac{\rho k^{3/2}}{\epsilon} \qquad (4)$$

where k and ϵ are obtained from the solution of their transport equations. The modeled forms of these equations, which were used in almost all the aforementioned engine application studies, are, respectively, as follows:

$$\frac{\partial k}{\partial t} + (\bar{U}^j k)_{,j} = -\overline{u^i u^j}\, \overline{U}_{i,j} + (g^{ij} \frac{\mu_t}{\rho} k_{,i})_{,j} - \epsilon \qquad (5)$$

$$\frac{\partial \epsilon}{\partial t} + (\overline{U^j \epsilon})_{,j} = -1.44\, \overline{u^i u^j}\, \overline{U}_{i,j} \frac{\epsilon}{k} + 0.83 (g^{ij} \frac{\mu_t}{\rho} \epsilon_{,i})_{,j} - 1.92 \frac{\epsilon^2}{k} \qquad (6)$$

where the model constants have been implemented directly into the equations.

With the constant diffusivity model (CDM), μ_t has to be prescribed. Guided by the results from the k-ϵ model, several values of μ_t were tried. Although a single time invariant value of μ_t could be found that gave results in good agreement with the measurements at a particular crank angle, the same value did not give comparable agreement at other crank angles. It is conceivable, however, that a time variant, spatially constant diffusivity would be a more appropriate way of using this type of model. At any rate, the results that will be presented using the CDM were obtained with a constant diffusivity value of 0.005 kg/ms. This value gave the best overall agreement with the measurements.

The RSM is based on the solution of transport equation for the Reynolds stresses.

The version of the model used in the present work was suggested by Launder et al. [14] and was used previously in [2]. According to [2], the modeled transport equation of the tensor component $\overline{u^i u^k}$ reads:

$$\frac{\partial \overline{u^i u^k}}{\partial t} + \overline{U^j (u^k u^i)}_{,j} = -\left(\overline{u^k u^i}\,\overline{U^i}_{,j} + \overline{u^i u^j}\,\overline{U^k}_{,j}\right) - 1.6\,\frac{\varepsilon}{k}\left(\overline{u^i u^k} - \frac{2}{3}\,g^{ik}k\right)$$

$$+ 0.76\left(\overline{u^k u^j}\,\overline{U^i}_{,j} + \overline{u^i u^j}\,\overline{U^k}_{,j} - \frac{2}{3}\,g^{ik}g_{mn}\,\overline{u^m u^\ell}\,\overline{U^n}_{,\ell}\right) -$$

$$0.18\left(g^{\ell k}\,\overline{U^i}_{,\ell} + g^{\ell i}\overline{U^k}_{,i}\right) - 0.11\left(g_{j\ell}g^{km}\,\overline{u^i u^\ell}\,\overline{U^j}_{,m} + g_{j\ell}g^{im}\,\overline{u^k u^\ell}\,\overline{U^j}_{,m} -\right.$$

$$\left.\frac{2}{3}\,g^{ik}g_{mn}\,\overline{u^m u^\ell}\,\overline{U^n}_{,\ell}\right) + \left[0.125\,\frac{\varepsilon}{k}\left(\overline{u^i u^k} - \frac{2}{3}\,g^{ik}k\right)\right.$$

$$+ 0.015\left(\overline{u^k u^j}\,\overline{U^i}_{,j} + \overline{u^i u^j}\,\overline{U^k}_{,j} - g_{j\ell}\,g^{km}\,\overline{u^i u^\ell}\,\overline{U^j}_{,m} +\right.$$

$$\left.\left. g_{j\ell}\,g^{im}\,\overline{u^k y^\ell}\,\overline{U^j}_{,m}\right)\right]\frac{k^{3/2}}{\varepsilon x_n} + \frac{k}{\varepsilon}\left(\overline{u^i u^\ell}\,\overline{(u^j u^k)}_{,\ell} + \overline{u^j u^\ell}\,\overline{(u^k u^i)}_{,\ell} +\right.$$

$$\left.\overline{u^k u^\ell}\,\overline{(u^i u^j)}_{,\ell}\right)_{,j} - \frac{2}{3}\,g^{ik}\,\varepsilon$$

where x_n is the normal distance to the nearest solid boundary. Together with the equations of the Reynolds stress components, a further tranport equation for ϵ is required to close the set of equations. This equation for ϵ is identical to Equation (6) except for the diffusion term (second term on the right hand side) which, within a RSM, would have a diffusion coefficient of $0.15\,\frac{k}{\epsilon}\,\overline{u^i u^j}$.

Differencing Scheme: The computer code used in the present study is a version of the code CONCHAS [13]. This code is based on a variant of the implicit-continuous-fluid-Eulerian technique developed by Harlow and Amsden [15], and is equipped with an arbitrary-Lagrangian-Eulerian mesh. Several modifications were made to the code to include, among other things, the differencing schemes SUDS and QUICK. Details on these two schemes can be found in [8] and [9], respectively.

From a Fourier series type of analysis, it is possible to show that the QUICK scheme is totally free of numerical diffusion. It can be shown from a similar type of analysis (see Lai [12]) that SUDS reduces dramatically errors arising from the skewness of the flow streamlines relative to the grid lines. These errors are the main contributors to numerical diffusion in multi-dimensional flows. One major problem, however, with both differencing schemes is that they are not unconditionally bounded (in the sense given by [16]). This arises because the fluxes of ϕ leaving any control volume may be based on ϕ values other than the ϕ value associated with the control volume under consideration. With QUICK there is a further reason for unboundedness, namely, that the scheme does not possess the transportive property (for a definition, see [16]).

The unboundedness problems associated with both QUICK and SUDS were found to cause no serious problems with the momentum calculations. Serious problems, however, did arise when solutions of the turbulence equations (i.e., the k-ϵ and Reynolds stress equations) were attempted. These problems were signaled by the appearance of a sharp decline in the values of the turbulence quantities at scattered locations in the flow field. Such locations always coincided with regions having large gradients of the turbulence quantities. In some extreme cases, the "sharp declines" eventually led to negative values for strictly positive quantities. To remedy this problem, the procedure used previously by [2], in conjunction with solving the Reynolds stress equations using SUDS, was adapted to QUICK. Briefly, the procedure entails using the more accurate differencing scheme (i.e., QUICK or SUDS) whenever the solution is bounded while reverting to a bounded scheme whenever indications of an unbounded solution appear (for more details, see [2]).

Engine Speed Scaling. It was noticed from previous calculations that computational times necessary to complete an engine cycle increased almost linearly with reductions in engine speeds. Since in the problem considered, the engine speed was low (200 r/min), the computational times were excessively large. It was, therefore, necessary to find ways of reducing these times.

The reason for the large computation times encountered at low engine speeds can be attributed to the point iteration scheme implied in the solution procedure and to the low Mach number resulting at these engine speeds. Hence, to reduce computational times without changing the solution procedure, it would be necessary to increase the Mach number. This can be achieved by either reducing the speed of sound and/or increasing the engine speed. Due to its simplicity, the latter alternative was selected. Needless to say, for the procedure to be successful, the flow pattern must be independent of speed, a matter which is discussed next.

The possibility of altering piston speeds without changing the flow pattern rests on the validity of the assumption of dynamic similarity of the flows at the various speeds. In the current application, the flow is expected to be dynamically similar if it is either independent of Mach and Reynolds numbers or when these numbers are somehow retained constant. Because the Mach number was maintained at fairly low values, it had no significant effect on the flow pattern. As for the Reynolds number condition, in general, turbulent flows in the vicinity of solid boundaries are influenced to some extent by the Reynolds number. However, by numerical testing in the present range of operation, it was found that the Reynolds number plays only a minor role. Hence, the assumption of dynamic similarity is then valid.

Operating, Initial and Boundar Conditions

The testing of the procedure was achieved by comparing the numerical results with the laser Doppler anemometer measurements made by Morse et al. [7]. The measurements were carried out in the axisymmetric piston cylinder assembly shown schematically in Figure 1. The assembly consists of a flat crowned piston, a transparent cylinder with 75 mm bore, a flat transparent cylinder head, and an axisymmetric intake/exhaust port. The valve seat annulus angle was 30° relative to the cylinder axis direction. Further details on the geometry of the assembly are shown in Figure 1. The piston was driven in simple harmonic motion at 200 revolutions per minute and with a stroke of 60 mm, the average piston speed (V) was 0.4 m/s. At this speed, the flow was claimed to be fully turbulent.

Measurements were reported by Morse et al. for a flow case with zero swirl and for two other cases with different levels of swirl. In the swirling flow cases, swirl was generated by swirl vanes placed upstream of the inlet port. The degree of swirl was expressed through a swirl number defined as the ratio of the angular momentum flux to the axial momentum flux at entry to the cylinder, normalized by the width of the jet. In the present comparisons, only the zero swirl flow and the flow with the higher swirl level were considered. In the latter flow, the swirl number reported by [7] was 1.2 (±10%).

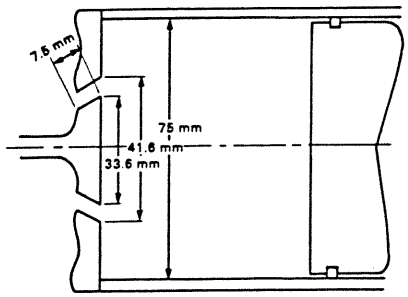

Figure 1. Schematic of Piston-Cylinder Assembly.

Morse, et al. presented all three components of mean and turbulent velocity for the swirling flow. For the non-swirling flow, only the axial mean and turbulent velocities were given. In all cases, velocity profiles were presented at several locations in the cylinder at crank angles of 36°, 90°, 144°, and 270° ATDC.

Except for two cases, all the calculations reported in the present work were conducted with a 45x45 computation grid. This mesh size was found to be sufficient to yield what appears to be a grid independent solution at crank angles of 36° and 90° ATDC. At 144°, similar calculations made in a previous study [2] revealed some sensitivity to grid size. Hence, comparisons between the models will not be conducted beyond 90° ATDC. Two computational runs were carried out with a 32x32 grid. These were used for comparing the accuracies of SUDS and QUICK. Although calculations with SUDS and QUICK were made both with the RSM and the k-ε model, only the results of the comparison using k-ε will be shown since both turbulence models yielded results leading to the same conclusions about the differencing schemes.

The computations were all carried out at an engine speed of 1200 r/min. However, because the results are presented in normalized form and dynamic similarity holds, the results are expected to be identical to computations made at 200 r/min. This was confirmed to be the case by some preliminary calculations. The saving in computer time by going to the faster speed was about a factor of 6.

Boundary Conditions. At solid boundaries, the following constraints were applied:

$$\vec{U}\cdot\vec{t} = 0,\ \vec{U}\cdot\vec{n} = U_b,\ D\left(\overline{u^i u^j}\right) = 0$$

where $\vec{t}$ and $\vec{n}$ are unit vectors in the direction tangent and normal to the boundary, u is the mean velocity vector, U_b is the velocity of the boundary, and $D(\ )$ signifies diffusion of the enclosed variables.

At intake, the flow is assumed to enter with a uniform velocity profile tangential to the valve-seat annulus at a volumetric rate equivalent to the rate displaced by the piston. In the presence of swirl, the swirl velocity profile is also assumed uniform. With this assumption, and with a swirl number of 1.2, we obtain a swirl velocity at entrance of about 0.26 the average inlet axial velocity. The turbulence kinetic energy at inlet was assumed equal to 2% of the kinetic energy based on mean inlet velocity. When the RSM is used, double the turbulent kinetic energy is distributed between the radial, azimuthal, and axial stress, respectively, as 0.5 k, 0.7 k, and 0.8 k. The dissipation rate was set to 0.5 k/(annulus width).

At the axis of symmetry, the radial velocity component is set to zero and fluxes of all other variables involved in transport equations are also set to zero.

In the computation carried out using the different turbulence models, all computational aspects were identical except for one difference. This difference is in the use of the logarithmic "law" of the wall. With the k-ε and CDM, the logarithmic law was used, while for reasons noted in [2], this law was not used with the RSM. It should be stated though that use of the logarithmic law made no apparent difference in the results obtained with the RSM up to 36° ATDC. The main difference, which is not very significant, was apparent beyond 70° ATDC.

Initial Conditions. In all the cases considered, computations were initiated from top dead center where the following conditions were assumed: the radial velocity and the axial velocity components were set equal to zero. In the presence of swirl, the profiles of swirl velocity normalized by mean

piston speed (U_θ) were assumed independent of axial location and to satisfy the following relations:

$$U_\theta \begin{cases} = \frac{3r}{R} & \text{when } r < 0.33\ R \\ = 1 & \text{when } 0.33\ R < r < 0.9\ R \\ = 2.7 \quad (R-r)/R & r > 0.9\ R \end{cases}$$

where r is the (variable) radius, and R is half the bore. The shape of the swirl profile is an approximation to the average swirl profile measured by [7] at 270° ATDC. The turbulence is assumed isotropic and has a kinetic energy approximately equal to 18% (see [2]) of the kinetic energy based on mean piston speed. The dissipation rate was calculated from:

$$\epsilon = 0.4\ k^{3/2} / \ x_n$$

RESULTS AND DISCUSSION

Global Flow Features

Before discussing the influence of the numerical scheme and turbulence on the results, a brief idea on the flow pattern generated in the two flow cases considered will first be given (more details may be found in [7]) at 90° ATDC for the non-swirling and swirling flows, respectively.

The flow in the non-swirling case (Figure 2a) is composed of a jet emanating from the intake port, surrounded by three vortices. A large vortex is evident residing on the center-line side of the jet which rotates clockwise. There is also a significantly smaller vortex occurring in the corner between the cylinder wall and cylinder head. The jet is seen to impinge on the cylinder wall and then to spread out in the direction of the piston. Close to the cylinder wall the flow separates and gives rise to a third vortex rotating anti-clockwise.

In the presence of swirl (Figure 2b), several variations to the flow field occur. Three of these differences are signficant. First, the larger vortex, which is adjacent to the center line, is seen to stretch in the presence of swirl in the direction of the piston. Second, a new recirculating zone is established below the valve. Finally, the vortex residing close to the piston and

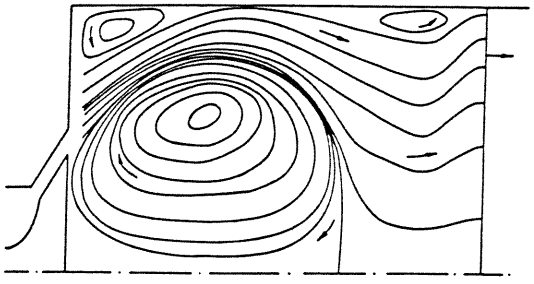

Fig. 2a. Stream-Line Contours of Non-Swirling Flow at 90° ATDC.

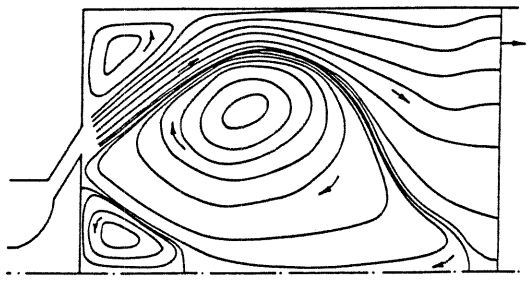

Fig. 2b. Stream-Line Contours of Swirling Flow at 90° ATDC.

cylinder wall corner almost disappears. All these effects accompanied by swirl can be explained by the action of centrifugal forces.

Figures 3a and 3b show the calculated velocity vector plots as 90° ATDC for the non-swirling and swirling flows, respectively. The plots, which were obtained by the RSM, are seen to reproduce the trends in the measured data fairly well.

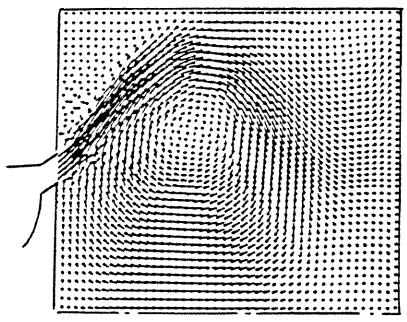

Fig. 3a. Velocity Vector Plot for Non-Swirling Flow at 90° ATDC.

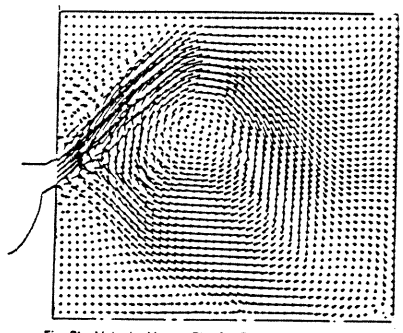

Fig. 3b. Velocity Vector Plot for Swirling Flow at 90° ATDC.

Comparison Between QUICK and SUDS

With the intent of comparing the performance of SUDS versus that of QUICK, computations were carried out with these schemes using both the k-ϵ model and the RSM for the non-swirling flow case. The conclusions reached from these computations, using either turbulence model at all crank angles, were similar and, hence, only the results at 90° using the k-ϵ model are presented.

Figure 4 shows measured and calculated mean axial velocity profiles at various loca-

tions in the flow field. In this and all following figures, the velocities are normalized by the mean piston speed (V) and are plotted relative to datums[2] (dashed lines perpendicular to the cylinder axis) at various distances from the cylinder head. It is clear from the figure that SUDS yields results in better agreement with the measured data than the results produced by QUICK. This is particularly the case at location 3. This finding was surprising since, based on a Taylor series analysis, SUDS is formally a first-order accurate scheme, while QUICK is second order. Furthermore, the experience of [10] and [11] suggests that the two differencing schemes are expected to yield similar results. There is, however, the following possible explanation for this anomaly.

In the present flow situation, the flow enters skewed at an angle of 30° relative to the vertical grid lines. This angle is further increased due to the entrainment by the jet of fluid with radially outward momentum (see Figure 2a). Now, it is plausible that as the skewness angle increases, the infringement on the transportive property by QUICK increases, thus compromising its accuracy. In the meantime, the accuracy of SUDS, as shown by [12], may actually increase at the larger skewness.

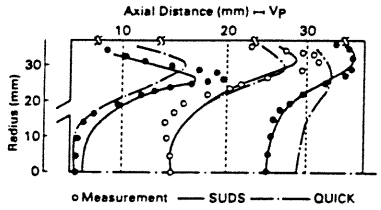

Fig. 4. Mean Axial Velocity Profiles at 90° ATDC.

In fairness to the QUICK scheme, it should be remarked that the present flow case is unsuitable for an assessment of the differencing scheme. This is because of uncertainties in the physical model and boundary conditions. However, since no other guidance is available, SUDS was considered more accurate than QUICK and was used in all the calculations to be presented. We next review the comparative study between the turbulence models.

Comparison Between Turbulence Models

Non-Swirling Flow. Figures 5 and 6 show measured and calculated mean axial velocity profiles at 36° and 90° ATDC, respectively. In these figures, two sets of calculations are presented - one made by the k-ε model and the other with the RSM. At 36° ATDC, the axial velocities predicted by the two models

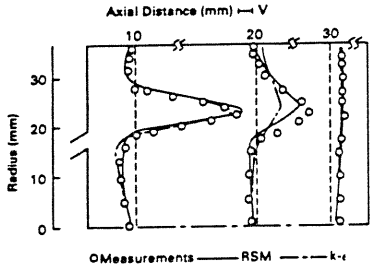

Fig. 5. Mean Axial Velocity Profiles at 36° ATDC (Non-Swirling Flow).

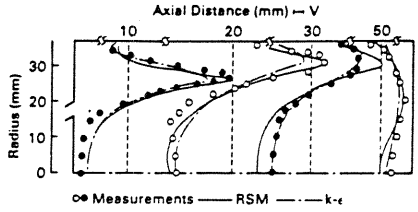

Fig. 6. Mean Axial Velocity Profiles at 90° ATDC (Non-Swirling Flow).

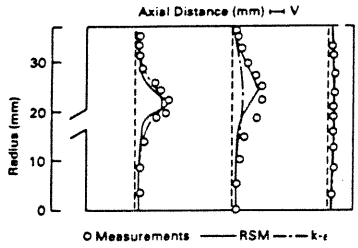

Fig. 7. Axial Turbulence Velocity Profiles at 36° ATDC (Non-Swirling Flow).

at locations 1 and 3 are seen to be in excellent agreement with the measurements. At location 2, the velocities calculated by the RSM are in fair agreement with the measurements, but the k-ε model tends to be quite diffusive with a consequence of underestimating the peak velocity by 50%.

At 90° ATDC the velocity profiles predicted by the two models reproduce most of the measured trends. Quantitatively, except at location 3, the peak velocities calculated by the RSM are in excellent agreement with the measurements. At location 3, however, the peak velocity is overestimated by about 35%. Although the k-ε model underestimates the peak velocities at locations 1 and 2 by about 25%, unexplainably it is in very good agreement with the measurements at location 3.

Profiles of the axial turbulence velocities[3] normalized by mean piston speed are shown in Figures 7 and 8 at 36° and 90° ATDC. At 36°, the agreement between trends and values of peak velocities measured and those predicted by the RSM is very good. However, in some regions, specifically those coinciding with the side edges of the jet, the predictions of the RSM somewhat underestimate the turbulence levels. With the k-ε model,

2. The locations of the datums shown will be referred to as location 1, 2, 3, etc., with location 1 being closest to the cylinder head and 2 the second closest, etc.

3. With the k-ε model, the axial turbulence velocity is taken equal to 2/3 k.

predictions at locations 1 and 3 are comparable to the predictions obtained with the RSM, but at location 2 the turbulence predicted by this model is grossly underestimated.

In Figure 8 (i.e., at 90° ATDC) at location 1 it is seen that the Reynolds stress model predicts the peak velocity to within 15%, but unlike the measurements, the calculated turbulent velocity falls sharply with increasing radii beyond the location of peak velocity. With the k-ε model, the peak velocity is within 30% from the measured peak, but the profile beyond the peak does not fall as rapidly as with the RSM. At the other location, the RSM performs better than the k-ε model, although it is not entirely satisfactory at location 2.

Swirling Flow. Figures 9, 10, and 11 show the axial, azimuthal (i.e., swirl), and radial mean velocity profiles at 36° ATDC. In these and all following figures for mean velocities, results obtained from the constant diffusivity model are included in the comparison.

The main features of the axial velocity profiles (Figure 9) are seen to have changed very little from the non-swirling flow case. The main differences are a slight reduction in peak velocities at locations 1 and 2, the shortening (in the axial direction) of the recirculating region present in the corner between the cylinder head and wall, and a reduction in the velocities near the center line. The level of agreement between experimental values, and values obtained with the k-ε and RSM models, is similar to that observed in the non-swirling case. As for the CDM, it is apparent that the model smears the jet region substantially. This is a consequence of the large diffusivity used which was necessary to yield good agreement with the measurements at 90° ATDC. Better agreement between the CDM results and the measurements was obtained when a lower diffusivity was used, but this was at the expense of worse agreement at 90° ATDC.

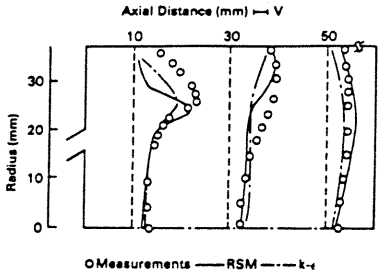

Fig. 8. Axial Turbulence Velocity Profiles at 90° ATDC (Non-Swirling Flow).

With the azimuthal velocity (Figure 10), all the predictions have the same trends as the measurements, but they underestimate the swirl velocity in almost the entire cylinder. This suggests that the total angular momentum present in the calculations is less than that

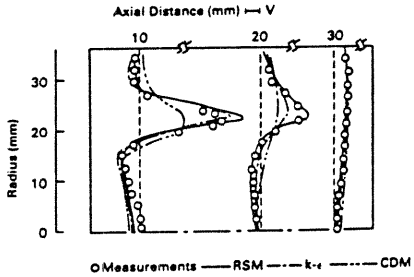

Fig. 9. Mean Axial Velocity Profiles at 36° ATDC (Swirling Flow).

which was inferred from the measurements. Since the amount of decay in angular momentum from TDC to 36° ATDC is small (≈2%), the reason for the under evaluation in swirl velocity can be attributed to incorrect boundary and/or initial conditions. The latter is more likely since the amount of mass present in the clearance volume is substantially larger than the mass inducted during the first 36° of induction.

In a similar manner to the swirl velocity prediction, the k-ε model and the RSM are seen (Figure 11) to be in agreement in their prediction of the mean radial velocity. Although the trends in these predictions are in agreement with those in the measurements, quantitatively, at certain locations in the flow field there are deviations. Thus, the predictions overestimate the velocity around mid-radius at location 2. Also, the radius at which peak velocity occurs at location 1 is underestimated. The deviations most probably are connected to the under-evaluation of the swirl velocity. With the CDM, the radial velocities calculated at locations 1 and 2 are quite different from those calculated with either the k-ε model or the RSM. This was to be expected because of the significantly different axial velocities calculated by CDM and the other models.

The axial velocity profiles at 90° ATDC are shown in Figure 12. The influence of the swirling motion on the flow pattern is now quite evident, particularly in regions near to the center line. Except for an overestimation of the size and strength of the vortex

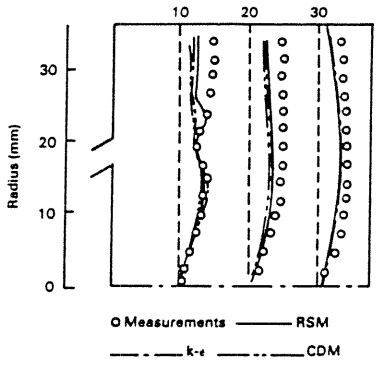

Fig. 10. Mean Azimuthal Velocity Profiles at 36° ATDC (Swirling Flow).

neighboring the cylinder head and center line, the RSM is in good agreement with the measurements. The k-ϵ model and, surprisingly, the CDM are also found to be in accord with the measurements.

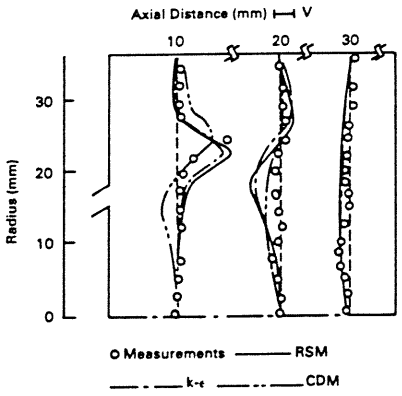

Fig. 11. Mean Radial Velocity Profile at 36° ATDC (Swirling Flow).

Figure 13 depicts the mean azimuthal velocity at 90° ATDC. The shape of the profiles have changed from the rather flat shape occurring at 36° ATDC. Here, the profiles at locations 3 and 4, and to some extent at location 2, exhibit bulges near the center line. These are caused by the radially inward (i.e., towards the center line) motion of the flow at the former two locations. In an effort to conserve its angular momentum, the fluid, in moving towards the center line, increases its swirling velocity. At location 2, the flow is radially outwards and it seems that the slight bulge there is caused by transport effects. Both the k-ϵ model and CDM are seen to exaggerate the bulges with the peak velocities in the bulges occurring at a larger radius than suggested by the measurements. With the RSM the swirl velocity in the bulges conforms more with the measurements. Away from the center line region and also at location 1, in agreement with the measurements, all the models predict relatively flat profiles.

The mean radial velocity profiles are shown in Figure 14. The level of agreement between the different models and the measurements vary depending on location. In general, the different models perform equally well with possibly the RSM and CDM showing closer agreement with the measurements.

The turbulence velocities are shown in Figures 15-17 consecutively for the axial, radial, and azimuthal components. In all these figures the turbulence velocity components calculated by the k-ϵ model are the same and equal to 2/3 k. The level of agreement between the axial velocities calculated by the RSM and the measurements is similar to the case for the non-swirling flow. Hence, the peak velocities are well predicted and away from the jet region the agreement is good. But, in the region flanking the peak velocity in the jet, the turbulence velocity is underestimated. With the k-ϵ model, again similar to what was observed for the non-swirling flow, the agreement with the measurement and the RSM is good at location 1 and 3, but the turbulence is significantly underestimated at location 2.

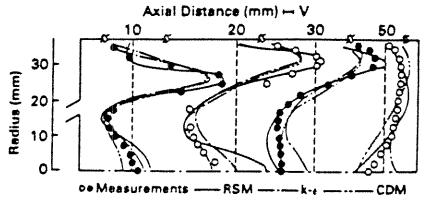

Fig. 12. Mean Axial Velocity Profiles at 90° ATDC (Swirling Flow).

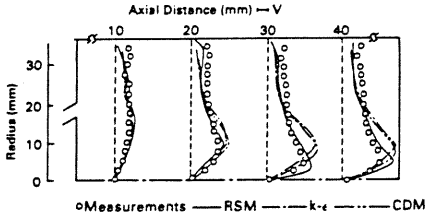

Fig. 13. Axiumthal Velocity Profiles at 90° ATDC (Swirling Flow).

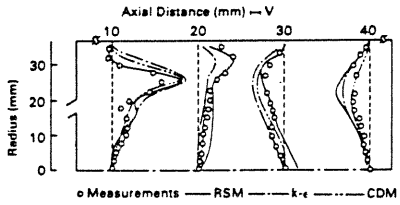

Fig. 14. Mean Radial Velocity Profiles at 90° ATDC (Swirling Flow).

As shown in Figure 16, both the k-ϵ model and the RSM can be used to calculate, at locations 2 and 3, azimuthal turbulence velocities in good agreement with the measurements. At location 1, only the RSM has good agreement with the measurements, while the k-ϵ model predicts larger velocities. As for the radial turbulence component shown in Figure 17, it can be seen that the overall trends predicted by the RSM and k-ϵ model agree with the measurements. Quantitatively, with the exception of location 1, again the two model results agree reasonably well with the measurements. At location 1, the measured peak component is much higher than those predicted. It is suspected, however, as discussed later, that this high value of peak velocity is due to an experimental error.

To give an idea on the degree of isotropy of turbulence in the flow field, the three turbulence components are superimposed in Figure 18. As expected, in the jet region the turbulence is anisotropic. The axial component in almost all of this region is significantly larger than either the radial or azimuthal components. At only a single location are the measured radial components seen to be larger than the measured axial component. This is at location 1 at a radius equal to about 0.34 times the bore. The

occurrence of this high value of the radial component is difficult to explain, and it seems that this peak might be an error in the measurements. Apart from the occurrence of the one high value of the measured radial component, the calculations made with the RSM reproduce the degree of anisotropy of the turbulence fairly well.

The three turbulence velocity components at 90° ATDC are shown in Figures 19-21. These components are overlaid in Figure 22. It is clear from these figures that, in general, the RSM is more accurate than the k-ε model in predicting the turbulence field at 90° ATDC. The only instance where the k-ε model is found to be in better agreement with the measurements is at the outer radii at location 1. There, the energy levels predicted by the k-ε model are higher and, hence, in better agreement with the measurements than those predicted by the RSM. This observation was found to occur with varying degrees in the two flows investigated at all crank angles. Because of the complexity of the flow and the limited amount of data available, it is difficult to identify with certainty the cause(s) as to why the turbulence calculated at location 1 with the RSM falls off rapidly in disagreement with the measurements beyond the location of maximum turbulence.

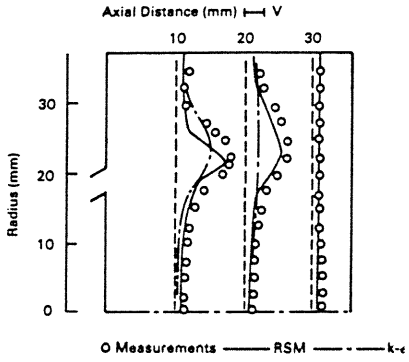

Fig. 15. Axial Turbulence Velocity Profiles at 36° ATDC (Swirling Flow).

SUMMARY AND DISCUSSION

To summarize the results obtained, both the k-ε model and the RSM were found to produce mean velocities in fairly good agreement with the measured velocities. The CDM, which was tested only for the swirling flow situation, could be made to yield good agreement with the measurements during only a specific range of crank angles during the induction stroke. Better agreement during the whole stroke could have possibly been obtained if the diffusivity were made to change with crank angle. It should be added though that the CDM is not entirely a prediction tool but has to be used in conjunction with either measured data or a more predictive model such as the k-ε model. This is because the diffusivity must be input to the model.

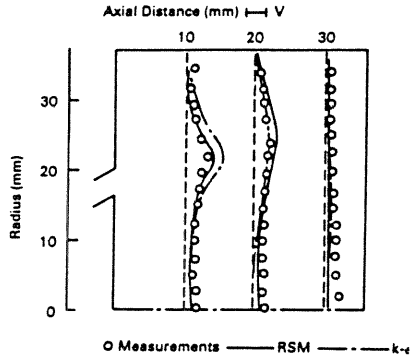

Fig. 16. Azimuthal Turbulence Velocity Profiles at 36° ATDC (Swirling Flow).

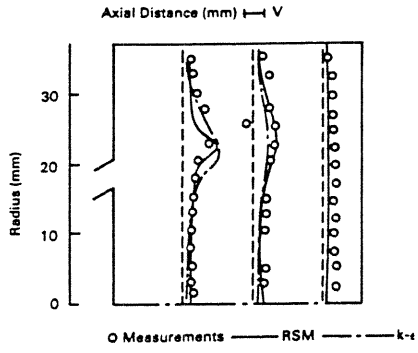

Fig. 17. Radial Turbulence Velocity Profiles at 36° ATDC Swirling Flow.

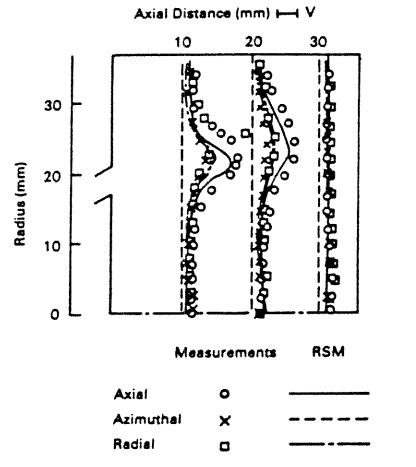

Fig. 18. Turbulence Velocity Profiles at 36° ATDC (Swirling Flow).

As for the turbulence field overall, the RSM predicted the energy levels in better accord with the measurement than the k-ε model. Furthermore, the RSM was capable of predicting realistic levels of the anisotropy

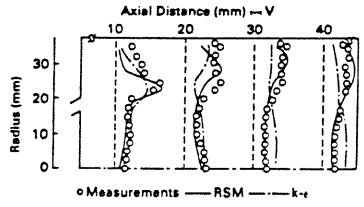

Fig. 19. Axial Turbulence Velocity Profiles at 90° ATDC Swirling Flow.

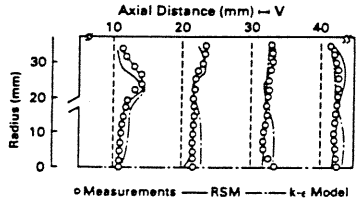

Fig. 20 Azimuthal Turbulence Velocity Profiles at 90° ATDC (Swirling Flow).

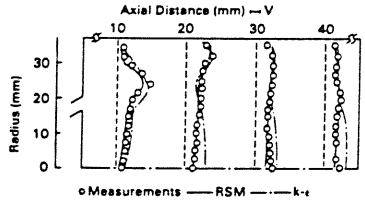

Fig. 21. Radial Turbulence Velocity Profiles at 90° ATDC. (Swirling Flow)

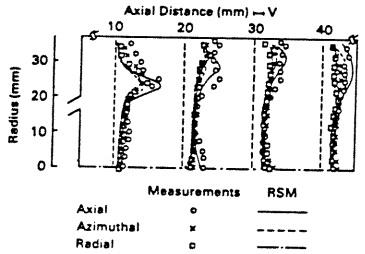

Fig. 22. Turbulence Velocity Profiles at 90° ATDC (Swirling Flow).

of the normal turbulence components. The k-ε model, on the other hand, in its present format, is incapable of such calculations. This capability may be seen as an academic one, particularly when the normal stresses play a minor role in driving the mean flow or in generating turbulence. However, it is a feature that may be important when considering scalar diffusion.

Although, as mentioned, the RSM has the advantage over the k-ε model of being a more comprehensive, and in some instances, more accurate representation of turbulence, it has its shortcomings. First, there is the problem of handling a much more complex set of equations. Second, there is the additional cost of storage and computer time involved in the solution of such equations. There are also some problems that arise in the solution of the momentum equations using the RSM. These problems are associated with velocity vector oscillations which are inherent in the solutions obtained by CONCHAS (see [2]); with the RSM, these oscillations are exacerbated.

REFERENCES

1. Mattavi, J. N. and Amann, C. A. (Eds.), Combustion Modeling in Reciprocating Engines, Plenum Press, New York, 1980.
2. El Tahry, S. H., "Application of a Reynolds Stress Model to Engine Flow Calculations," GM Research Report FM-2/EN-295, June 16, 1983.
3. Gosman, A. D., Johns, R. J. R., and Watkins, P. A., "Development of Prediction Methods for In-Cylinder Processes in Reciprocating Engines," Combustion Modeling in Reciprocating Engines, Ed. J. N. Mattavi and C. A. Amann, Plenum Press, New York, 1980, p. 69.
4. Diwakar R. and El Tahry, S. H., "Comparison of Computed Flow-Field and Wall Heat Fluxes with Measurements from Motored Reciprocating Engine-Like Geometries," presented at ASME Third International Computer Engineering Conference, August 1983.
5. Ahmadi-Befrui, B., Arcoumnis, C., Bicen, A. F., Gosman, A. D., Jahanbakhsh, A. and Whitelaw, J. H., "Calculations and Measurements of the Flow in a Motored Model Engine and Implications for Open-Chamber Direct-Injection Engines," Imperial College, Mechanical Engineering Department Report FS/81/34, October 1981.
6. Ramos, J. I., Gany, A., and Sirignano, W., "Study of Turbulence in a Motored Four-Stroke Internal Combustion Engine," AIAA, Vol. 19, p. 595, 1981.
7. Morse, A. P., Whitelaw, J. H. and Yianneskis, M., "Turbulent Flow Measurements by Laser-Doppler Anemometry in a Motored Reciprocating Engine," Imperial College Mechanical Engineering Department Report FS/78/24, 1978.
8. Raithby, G. D., "Skew Upstream Differencing Schemes for Problems Involving Fluid Flow," Computer Methods in Applied Mechanics and Engineering, Vol. 9, p. 153, 1975.
9. Leonard, B. P., "A Stable and Accurate Convective Modeling Procedure Based on Quadratic Upstream Interpolation," Computer Methods in Applied Mechanics and Engineering, Vol. 19, p. 59, 1979.
10. Leschziner, M. A., "Practical Evaluations of Three Finite Difference Schemes for the Computation of Steady-State Recirculating Flows," Computer Methods in Applied Mechanics and Engineering, Vol. 23, p. 293, 1980.
11. Leschziner, M. A. and Rodi, W., "Calculation of Annular and Twin Parallel Jets Using Various Discretization Schemes and Turbulence-Model Variations," J. of Fluids Engineering, Vol. 103, p. 352, 1981.
12. Lai, K. Y. M., "Numerical Analysis of Fluid Transport Phenomena," Ph.D. Thesis, University of London, 1982.

13. Butler, T. D., Cloutman, L. D., Dukowicz, J. K., and Ramshaw, J. D., "CONCHAS: An Arbitrary Lagrangian-Eulerian Computer Code for Multi-Component Chemically Reactive Fluid Flow at All Speeds," Los Alamos Scientific Laboratories Report LA-8192-MS, 1979.

14. Launder, B. E., Reece, G. J., and Rodi, W., "Progress in the Development of a Reynolds-Stress Turbulence Closure," J. Fluid Mech., Vol. 68, p. 537, 1975.

15. Harlow, F. H. and Amsden, A., "A Numerical Fluid Dynamics Calculation Method for All Flow Speeds," J. of Comput. Phys., Vol. 8, p. 197, 1971.

16. Roache, P. J., Computational Fluid D namics, Hermosa Pulishers, Albuquerque, 1972.